

Using hyperspectral and thermal imagery to monitor stress of Southern California plant species during the 2013–2015 drought

Susan K. Meerdink ^{a,b,c,*}, Dar A. Roberts ^c, Jennifer Y. King ^c, Keely L. Roth ^d, Paul D. Gader ^b, Kelly K. Taylor ^c

^a Department of Geographical and Sustainability Science, University of Iowa, Iowa City, IA 52242, United States

^b Engineering School of Sustainable Infrastructure and Environment, University of Florida, Gainesville, FL 32611, United States

^c Department of Geography, University of California Santa Barbara, Santa Barbara, CA 93106-4060, United States

^d Planet Labs, San Francisco, CA 94103, United States



ARTICLE INFO

Keywords:

Thermal
Drought
Species
Hyperspectral
HypSIRI Airborne Campaign
Surface Biology and Geology (SBG)

ABSTRACT

From 2012 to 2015, California experienced the most severe drought since 1895, causing natural vegetation throughout the state to become water-stressed. With many areas in California being inaccessible and having extremely rugged terrain, remote sensing provides a means for monitoring plant stress across a broad landscape. Airborne hyperspectral and thermal imaging captured the drought in the spring, summer, and fall seasons of 2013 – 2015 across 11,640 km² of Southern California. Here we provide a large-scale analysis of plant species' annual and seasonal temperature variability throughout this prolonged drought. We calculated the Temperature Condition Index (TCI) using airborne thermal imagery and a plant species classification map derived from airborne hyperspectral imagery to track response in three dominant species (e.g., Mediterranean grasses and forbs, chamise, and coast live oak) that have different stress adaptation strategies. The annual grasses and forbs showed strong seasonal changes in TCI, which corresponded to the typical green-up, peak biomass in summer, and senescence in the fall. They also had the strongest change in TCI values as the drought progressed from 2013 to 2015, with the months of April and August showing the most pronounced changes. The deeper rooted, native chamise evergreen shrub and coast live oak evergreen, broadleaf tree showed a more minor shift in seasonal and yearly patterns of TCI, but even these very well adapted species showed an increased amount of TCI stress as the drought progressed from 2013 to 2015. Across the study area and image dates, TCI stress was not evenly distributed, and in August 2015 almost the entire region experienced elevated TCI stress. To better understand the environment's effect on plant stress, we relate topographic attributes to plant stress. Higher TCI values correlated with south or south-southwest facing slopes, while other topographic attributes were weakly correlated with TCI. An increase in elevation had a strong correlation with a decrease in TCI stress, but this relationship weakened as the drought progressed. The synergistic capabilities of hyperspectral and thermal imagery demonstrate that we can monitor the dynamic nature of plant species' stress temporally and spatially. This work supports improved monitoring of natural landscapes and informing management possibilities, especially for areas prone to continued drought and high risk of wildfires.

1. Introduction

From 2012 to 2015, California experienced conditions that resulted in the most severe drought over the past 1200 years based on paleoclimate reconstructions (Griffin and Anchukaitis 2014). During these four years, the state's 12-month accumulated precipitation was less than 34 % of average, resulting in the hottest and driest annual conditions recorded since 1895 (Swain 2014; Mann and Gleick 2015). The resulting

water shortage led to a wide range of impacts on natural systems, including tree mortality (Young et al. 2017), bark beetle infestation (Tane et al. 2018; Guarín and Taylor 2005), and canopy water content loss (Asner et al. 2016). Extreme events, such as this drought, are projected to become more frequent and intense with the advance of climate change (Mastrandrea and Luers 2012; Mastrandrea et al. 2011; Mann and Gleick 2015). Monitoring vegetation health status provides valuable ecological information and ultimately guides management decisions

* Corresponding author.

E-mail address: susan-meerdink@uiowa.edu (S.K. Meerdink).

(Blossey 1999). However, the size or inaccessibility of management areas often makes tracking infeasible through ground efforts alone.

Thermal remote sensing has been used to track vegetation responses that are highly correlated with water availability in the environment or plant. At the plot level, researchers working on agriculture applications have been utilizing the relationship between plant temperature and water stress for five decades to improve irrigation techniques and increase crop yields (Jackson et al., 1977). This focus has resulted in the development of various indices still commonly used today, including the Crop Water Stress Index (Idso et al. 1981; R. D. Jackson et al. 1981), Degrees Above Non-Stressed Canopy (Taghvaeian et al. 2014), and the ratio of canopy temperature to non-stress crop (Bausch et al., 2011). These indices have been successfully used to manage irrigation practices (Thomson et al. 2012), but they generally require in-situ meteorological data or previously derived stress baselines. Additionally, because they have been developed for agricultural fields, the studies predominantly use handheld infrared thermal radiometers or unmanned aerial vehicles (UAVs) with mounted infrared thermal imaging to collect data (Costa, Grant, and Chaves 2013). Due to these prerequisites, these methodologies cannot be easily scaled for natural landscapes that are inaccessible and cover thousands of square kilometers.

To monitor vegetation stress at larger scales, researchers quantify stress using temperature calculated from spaceborne sensors such as the Advanced Very High Resolution Radiometer (AVHRR), the Moderate Resolution Imaging Spectroradiometer (MODIS), or the Landsat Enhanced Thematic Mapper (ETM+). The use of these sensors has resulted in the development of temperature-based indices for monitoring drought, such as the Temperature Condition Index (Felix N. Kogan 1997; F. N. Kogan 1995) and indices based on a combination of temperature and vegetation index, such as the Vegetation Temperature Condition (Wan, Wang, and Li 2004), the Vegetation Health Index (Felix N. Kogan 1997; F. Kogan et al. 2004), and the Drought Severity Index (Bayarjargal et al. 2006). These indices have been used to capture plant water stress during droughts in many places, including India (Bhuiany et al., 2006; Sruthi and Aslam 2015; Singh et al., 2003), the United States (Wan, Wang, and Li 2004; F. N. Kogan 1995), and Mongolia (Karnieli et al. 2006; F. Kogan et al. 2004; Bayarjargal et al. 2006). With spatial resolutions of 1 km or coarser, these studies generally focus on global or large regional patterns of plant stress. While Landsat's land surface temperature product is downsampled to 30 m, providing the ability to examine temperature responses on a finer scale, the multi-spectral nature of Landsat limits the ability to explore patterns at anything more detailed than land cover types. Tracking responses or changes in land cover type has provided insights that can be leveraged for drought severity monitoring prediction purposes (Taiwo et al. 2023; Nichol and Abbas 2015). However, it does not provide an understanding of the health or resilience of the ecosystem which is dictated by the composition of species and their unique adaptation strategies (Jacobsen et al. 2007; Tyler et al., 2006).

Here, we explored how simultaneously collected airborne thermal and hyperspectral could enable the measurement of species stress trends. Very few studies have explored the combination of hyperspectral and thermal measurements, but those that have shown that the synergies can provide greater insight than one measurement alone (D. A. Roberts et al. 2015; Wetherley et al., 2018; Coates et al. 2015; Meerdink et al. 2016). Here, we leverage these synergies to provide an analysis into species response across a drought as measured by land surface temperature, which could be leveraged to assess ecological health or status in a wildfire prone area. Coincident hyperspectral and thermal datasets are available through the NASA Hyperspectral InfraRed Imager (HypIRI) airborne campaign, which captured Southern California's extreme drought conditions during the 2013–2015 spring, summer, and fall seasons (Lee et al. 2015). Tracking landscape vegetation stress is well established, but with the combination of hyperspectral and thermal data, we can track individual species' stress across time, providing greater insight into plant response across different adaptation strategies.

We evaluate three dominant species' responses during California's recent drought across 11,640 km² of Southern California for nine dates during the years 2013 to 2015 using hyperspectral data to classify species and thermal to calculate the temperature condition index (TCI). Specifically, we created maps of an evergreen broadleaf chaparral shrub (chamise, *Adenostoma fasciculatum*), an evergreen broadleaf tree (coast live oak, *Quercus agrifolia*), and annual Mediterranean grasses/forbs stress, which enables the ability to ask what spatial and temporal patterns of stress are expressed across a landscape and how those responses vary with topographic factors.

2. Methods

2.1. Study area

The study area includes 11,640 km² in Southern California, where the majority is part of the Los Padres National Forest (LPNF), and the remainder is privately owned land or urbanized (Fig. 1). The elevation increases from sea level to a peak of 2,697 m, with the imagery capturing the transition from chaparral shrubland to conifer forests located in the LPNF. The study area is comprised of three ecoregion provinces: 1) chaparral forest and shrub, 2) open woodland, shrub, coniferous forest, and meadow, and 3) Sierran steppe-mixed forest, coniferous forest, and alpine meadow. The majority of the study area falls into the open woodland, shrub, coniferous forest, and meadow ecoregion province (McNab and Avers 1996). This ecoregion has elevation ranges from 153 to 3,496 m with narrow ranges and broad fault blocks, alleviated lowlands, and dissected westward sloping granitic uplands. Rivers and streams are common, but most do not flow throughout the year. Predominant natural communities include Chamise, Ceanothus, Mixed Chaparral, Scrub Oak, Coast Live Oak, Englemann Oak, Needlegrass, Jeffrey Pine, Canyon Oak, and Big Cone Douglas-Fir series. The next most prevalent ecoregion province for this study area is the chaparral forest and shrub, which has narrow ranges and broad fault blocks with elevations from sea level to 912 m (McNab and Avers 1996). There are very few perennial streams, and intermittent streams occur in alluvial and weak bedrock channels that flow directly into the Pacific Ocean. Predominant natural communities are Coastal Sage and Coastal Perennial Grassland series. The last ecoregion province is the Sierran steppe-mixed forest, coniferous forest, and alpine meadow. This covers the northeast portion of the study area with elevations ranging from 152 to 1064 m (McNab and Avers 1996). This area has many rapidly flowing rivers and streams that flow through deeply incised canyons. Predominant natural communities are Blue Oak, Interior Live Oak, Valley Needlegrass, and Mixed Chaparral series.

The entire study area experiences a Mediterranean climate characterized by cool, wet winters and hot, dry summers. Annual precipitation for the area ranges from 250 to 1000 mm, with 95 % falling between November and March (Diamond et al. 2013; Davis and Michaelsen 1995). However, during the time period studied (2013–2015), this area experienced extreme drought, with Santa Barbara County receiving 40 to 69 % of average rainfall (Griffin and Anchukaitis 2014; Swain 2014). Fig. 2 shows the daily precipitation for 2013–2015 at three stations: Santa Barbara Airport (elevation 2.7 m), Gibraltar Dam (elevation 475 m), and Pine Mountain Club (elevation 1834 m). The locations of these three stations are shown in Fig. 1. This area is also characterized by frequent wildfires that have been increasing in severity (Moritz 1997; Davis and Michaelsen 1995; Syphard et al., 2011). The LPNF has been actively suppressing wildfires since the 1900s, but suppression efforts became more effective after 1950 due to the use of large air tankers (Davis and Michaelsen 1995). Even with fire suppression, the time since the last fire is less than ten years for a large portion of the LPNF, although some areas have not burned in 75 or more years. The U.S. Drought Monitor reported an abnormally dry intensity (D0 rating) in April 2013 for this study. This increased to an intensity of severe drought (D2 rating) in June 2013, and the year ended with an intensity of

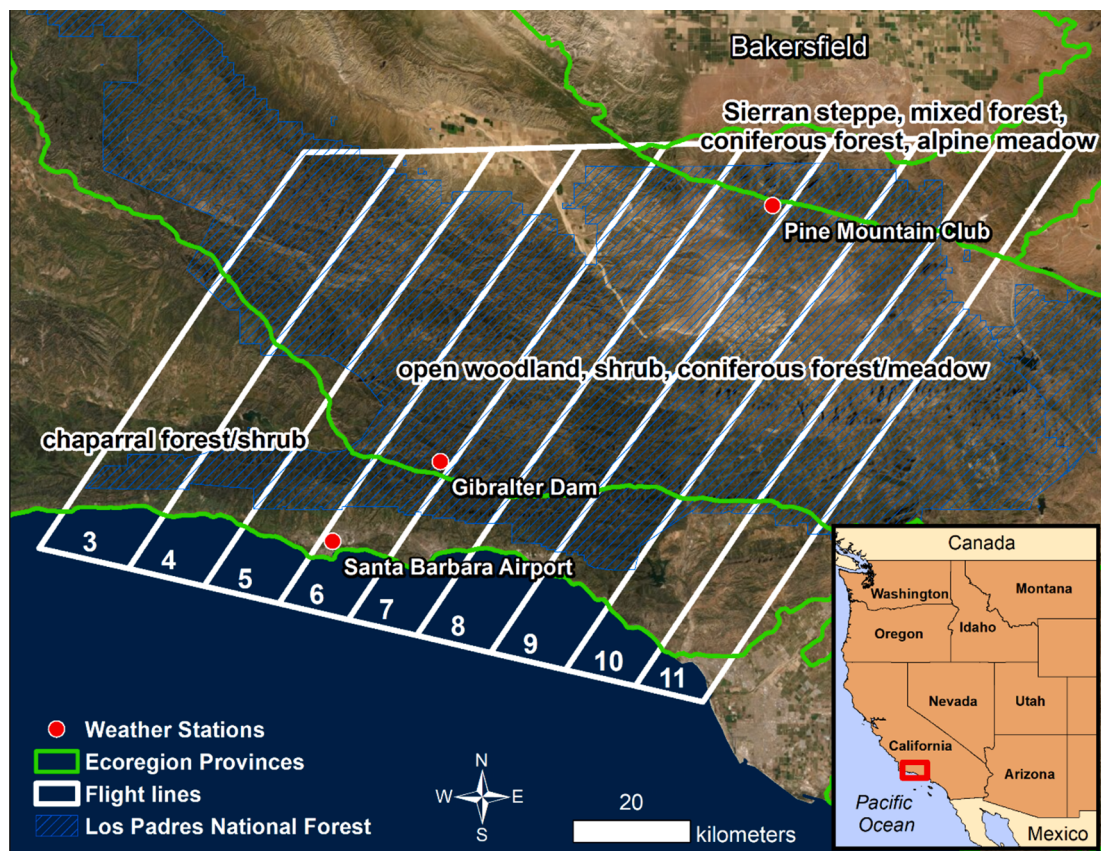


Fig. 1. The flight lines (white) and ecoregion provinces (yellow-green) in the Santa Barbara flight box used from the HyspIRI Airborne Preparatory campaign. (For interpretation of the references to colour in this figure legend, the reader is referred to the web version of this article.)

extreme drought (D3 rating) in November 2013. Starting in early 2014, the U.S. Drought Monitoring reported an intensity rating of exceptional drought (D4 rating) which persisted for the rest of this study's time period. The U.S. Drought monitoring ratings are included in Fig. A1.

2.2. Remotely sensed data

Remotely sensed imagery of the study area was collected with the Airborne Visible/Infrared Imaging Spectrometer (AVIRIS) and MODIS-ASTER Airborne Simulator (MASTER) sensor as part of the NASA HyspIRI Airborne Preparatory Campaign (Green et al. 1998; Hook et al. 2001). These sensors were flown simultaneously on the NASA ER-2 aircraft at an altitude of 20 km over six flight boxes in California to simulate future satellite imagery from HyspIRI (Lee et al. 2015). This study uses a spatial subset of imagery from the Santa Barbara flight box that includes nine of the eleven flight lines that were acquired with a 35° northeast-southwest orientation (Fig. 1). The imagery was collected in 2013 (Apr 11, June 6, Nov 23), 2014 (Apr 16, June 6, Aug 29), and 2015 (Apr 16, June 2, Aug 24). Some flight lines were excluded or replaced due to technical errors when collecting the data, resulting in 79 AVIRIS and 79 MASTER images being used in the analysis presented here. NASA's Jet Propulsion Laboratory (JPL) provided HyspIRI-like AVIRIS and MASTER products. For AVIRIS, this entails HyspIRI simulated reflectance products measuring 224 bands between 0.38 and 2.5 μ m with an 18 m spatial resolution (Thompson et al. 2015). For MASTER, the product was delivered with five emissivity bands and a land surface temperature band at a 36 m spatial resolution (Hook et al. 2001; Gillespie et al. 1998; Hulley and Hook 2011). The land surface temperature retrievals have an overall accuracy of ≤ 0.33 K and a noise equivalent differential temperature (NEdT) ranging from 0.15 – 0.74 K per band (Hulley and Hook 2011). Flight paths were optimized for 1 milliradian

AVIRIS instantaneous field of view resulting in significant overlap in MASTER flightlines because MASTER has an instantaneous field of view of 2.5 milliradian. Consequently, most areas had two to three land surface temperature measurements each from a different flightline, which captured temperature changes across the data collection day.

A series of additional pre-processing steps were required to use AVIRIS and MASTER datasets together across flight dates. AVIRIS products underwent additional pre-processing steps detailed in Meerdink et al., 2019. MASTER images were georeferenced to correct locational errors of the entire multi-temporal image sequences. The National Agriculture Imagery Program (NAIP) digital orthophotos, acquired in the spring and fall of 2012, were used as a reference source for the world coordinates. These orthophotos were mosaicked and resampled to 36 m spatial resolution for MASTER and used to collect ground control points. After pre-processing AVIRIS and MASTER images, the AVIRIS and MASTER images were layered into a single file. With an AVIRIS swath width of ~ 12 km and a MASTER swath width of ~ 40 km, any spatial areas not covered by both sensors were removed. The majority of clouds were masked out using a cloud spectral index that leveraged the hyperspectral optical bands and the MASTER thermal bands (Zhai et al. 2018). Through this process, we also masked shadowed pixels, as land surface temperature will be highly impacted by shadows. Some cirrus clouds remained in the image, specifically the April 2013 image which can be seen with lower TCI values on the lower, left portion of the image (Fig. 3).

2.3. Plant species information

Here, we focus on three dominant species on this landscape that represent different adaptive strategies: chamise (*Adenostoma fasciculatum*), coast live oak (*Quercus agrifolia*), and annual grasses/forbs.

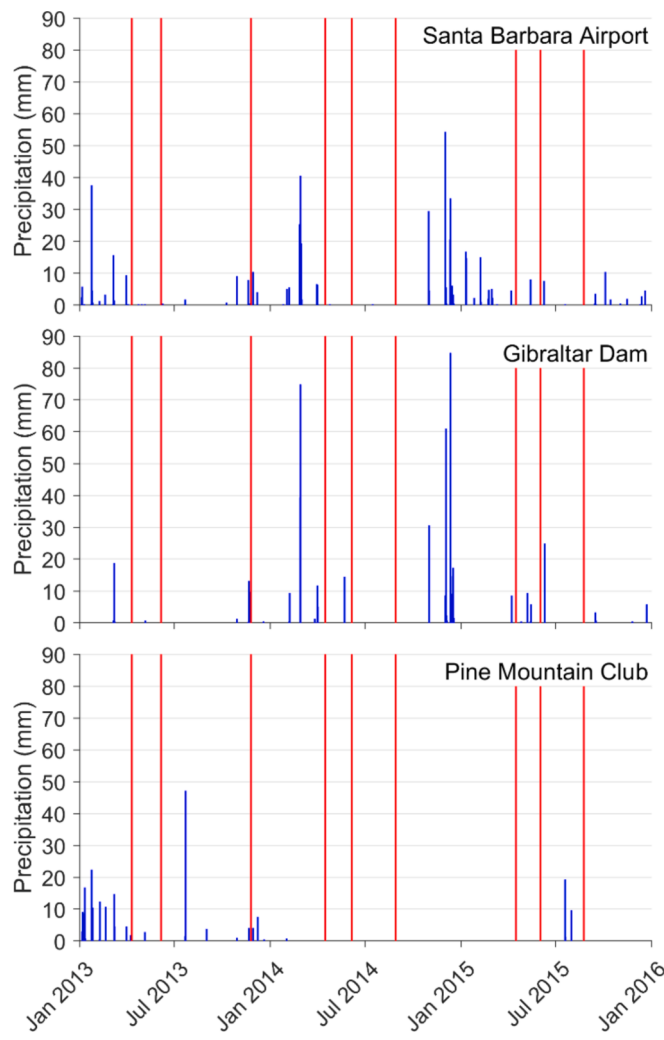


Fig. 2. Daily precipitation (blue) from January 2013 to January 2016 for three weather stations in the study area. The locations of the three stations are in Fig. 1. Red lines designate flight dates: 2013 Apr 11; 2013 June 6; 2013 Nov 23; 2014 Apr 16; 2014 June 6; 2014 Aug 29; 2015 Apr 16; 2015 June 2; and 2015 Aug 24. (For interpretation of the references to colour in this figure legend, the reader is referred to the web version of this article.)

Chamise is the dominant shrub species in this Mediterranean-climate ecosystem (Barbour, Keeler-Wolf, and Schoenherr 2007), which has adapted to rapid regrowth after fire by sprouting and seeding (Moreno and Oechel 1991). Chamise has a greater rooting depth for access to deeper water, but the roots are of small diameter (Hellmers et al. 1955). Coast live oak is an evergreen tree that can live for several hundred years. Coast live oak is drought evading and grows in areas relatively mesic with longer water availability with dense shade canopies to have a better advantage in low water and nutrient environments (Knops and Koenig 1994). Annual Mediterranean grasses have become the dominant species in California grasslands, replacing native perennial and annual grasses (L. E. Jackson 1985). For Mediterranean annual grasses and forbs, the start and end of the growing season are entirely dictated by rainfall patterns (Xu and Baldocchi 2004; Barbour, Keeler-Wolf, and Schoenherr 2007), with peak biomass generally occurring during late spring when most of the available soil moisture has been used, followed by full senescence by late summer (Becchetti et al. 2016).

The plant species classification used to extract species temperature values was developed using linear discriminant analysis and fine-tuned for each of the nine image dates. To train the model we used 1200 polygons of dominant species and land cover types that were developed

in the field with a spotting scope and using NAIP imagery (Meerdink et al. 2019). Spectra of each training polygon were extracted from each AVIRIS image date and underwent dimensionality reduction using canonical discriminant analysis. These field-validated training sets were split into 70 % for training and 30 % for validation over 50 iterations of model development. The canonical discriminant analysis spectral libraries split into training and validation were classified using linear discriminant analysis (Meerdink et al. 2019). In this work, we found that classification accuracies for species varied between the nine image dates due to the AVIRIS image quality and reduced spectral differences due to captured phenology. In this study area, no large events, such as wildfires or debris flows, occurred during this time period. So here we selected the plant species classifications with the highest accuracies (accuracies > 0.8 kappa), which included April 2013 (0.85 kappa), June 2013 (0.84 kappa), April 2014 (0.84 kappa), April 2015 (0.83 kappa), and June 2015 (0.86 kappa). From these five dates, we created a single plant species classification map by selecting a pixel's classification through majority voting across the five dates. So, if a pixel was classified as chamise in April 2013, April 2014, and April 2015, but classified as ceanothus for in the June 2013 and 2015 classifications, it was labeled as chamise in the classification map used in this study. This classification map was resampled to 36 m spatial resolution to match MASTER spatial resolution using the mode for pixels to be aggregated.

2.4. Temperature products

It is common in the literature to use land surface temperature minus air temperature as a proxy for plant stress (Vidal and Devaux-Ros 1995; Vidal et al. 1994; Moran et al. 1994). Ideally, air temperature should be included to fully characterize the impacts since air temperature is tied to convective processes while surface temperature is tied to radiative emission. However, this study area had an insufficient number of ground station measurements to robustly incorporate air temperature into the analysis. The Temperature Condition Index (TCI) has been used successfully to monitor drought-related vegetation stress in India, Mongolia, the United States, and globally (Felix N. Kogan 1997; F. N. Kogan 1995; Bhuiyan, Singh, and Kogan 2006; Singh, Roy, and Kogan 2003; Bayarjargal et al. 2006). TCI was chosen over other satellite-based indices because TCI ensured that temperatures across dates could be compared. This index was initially developed for the Advanced Very High-Resolution Radiometer (AVHRR) and uses brightness temperature from 1985 to 1993. We have altered the index for MASTER imagery over the nine image dates of this study. TCI was calculated for each species as:

$$TCI = 1 - \frac{(T_{max} - T)}{(T_{max} - T_{min})}$$

where T_{max} and T_{min} were the maximum and minimum surface temperature value over the nine image dates, and T was the surface temperature for each pixel. TCI was applied to each flightline. Given that the HyspIRI flight campaign path was designed for the AVIRIS sensor's field of view which is smaller than MASTER's field of view, there is significant overlap in the flightlines. The study region maps of TCI distribution were generated by finding the median TCI value for each pixel in the overlap region.

2.5. Topographic calculations

To determine which topographic attributes are associated with stressed plants, nine topographic attributes were calculated for correlation analysis with TCI distributions (Table 1; Fig. A2). Calculations of topographic attributes used the National Elevation Dataset (NED) from 2012, which is a ~ 10 m spatial resolution raster product assembled by the United States Geological Survey. The NED was used to calculate elevation in meters, slope in percent, and aspect in degrees. The elevation product was used to calculate the terrain ruggedness index (TRI),

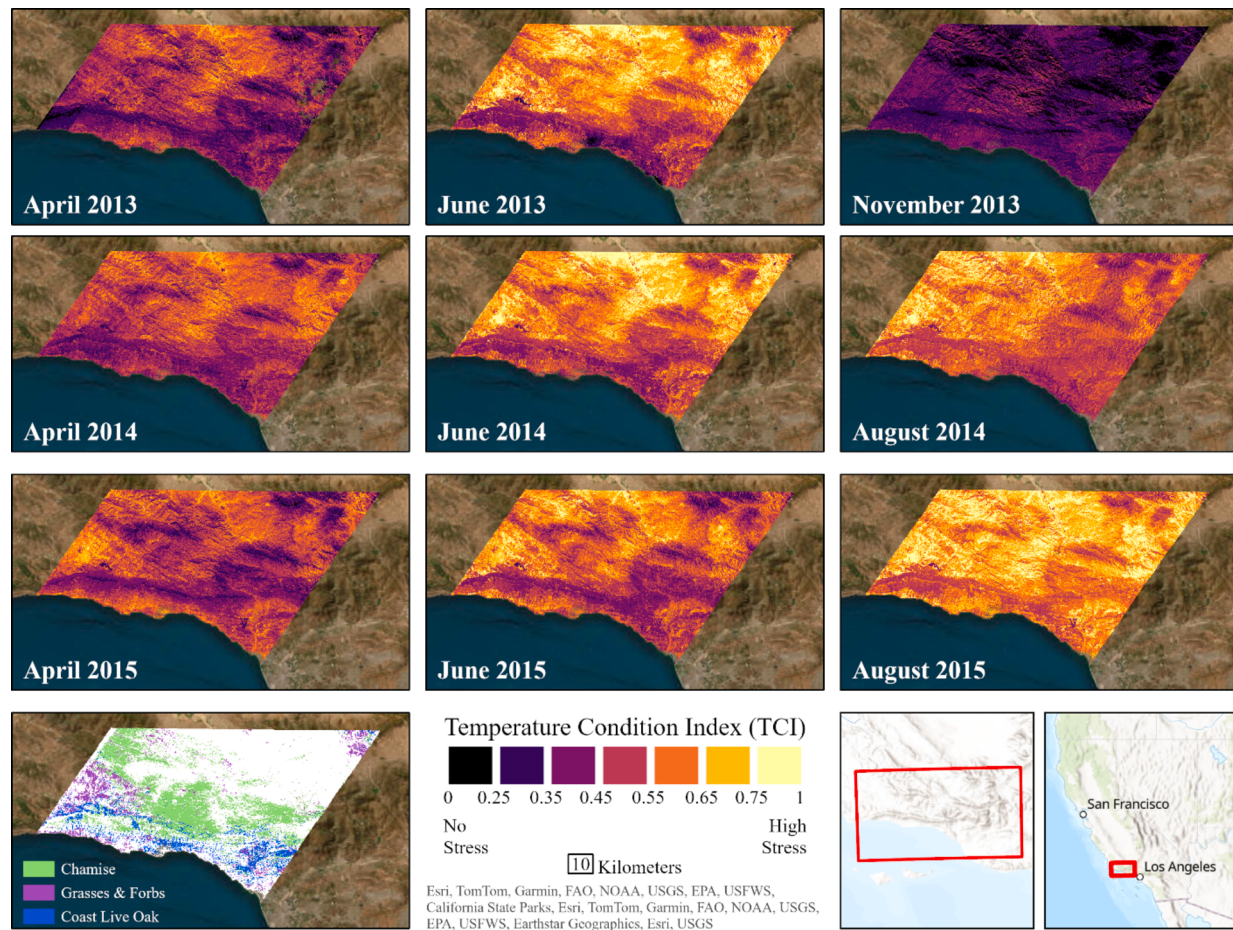


Fig. 3. Temperature condition index (TCI) calculated from the MASTER imagery, an airborne thermal sensor, for 2013 (top row), 2014 (second row), and 2015 (third row) with imagery from April (first column), June (second column), and November/August (third column) dates. In the bottom left corner is the distribution of chamise, grasses & forbs, and coast live oak determined from classifications using AVIRIS imagery, an airborne hyperspectral sensor.

Table 1

Topographic attributes extracted from the National Elevation Dataset and used for correlation analysis. α is the aspect in radians, and θ is the percent slope. For TRI, x_{ij} is the elevation of each neighbor cell to the center cell of the kernel (x_{00}). For TWI, A_s is the specific catchment area, and β is the slope. For more details, see Section 2.6.

Metric	Full Name	Formula
Elevation	Elevation (m)	
Slope	Slope (%)	
TRI	Terrain Ruggedness Index	$\left[\sum ((x_{ij} - x_{00})^2) \right]^{\frac{1}{2}}$
TWI	Topographic Wetness Index	$\ln\left(\frac{A_s}{\tan\beta}\right)$
N-S	North-south slope orientation	$\cos\alpha$
W-E	West-east slope orientation	$\sin\alpha$
NNE-SSW	North-northeast – south-southwest orientation	$\cos(\alpha - 30)$
N-S A + S	Cosine Transformation	$\theta^* \cos\alpha$
W-E A + S	Sine Transformation	$\theta^* \sin\alpha$
NNE-SSW A + S	Cosine Transformation with North-northeast – south-southwest orientation	$\theta^* \cos(\alpha - 30)$

which provides a quantitative measure of topographic heterogeneity (Riley, DeGloria, and Elliot 1999). For each pixel, the TRI value is calculated by the total change in elevation between a grid cell and its eight neighbor pixels. The elevation and slope products were used to calculate the topographic wetness index (TWI), which is commonly used to quantify topographic control on hydrological processes (Beven and

Kirby 1979). Using ArcGIS, a flow direction raster was calculated using elevation derived from NED. The flow direction raster was then used to calculate the flow accumulation raster, which finds the upslope contributing area for each pixel. TWI was then calculated using the flow accumulation and slope raster, adjusted by spatial resolution.

While elevation and slope were used directly in the correlation, the aspect variable was not because it is expressed as circular degrees clockwise from 0° to 360° ; thus, it is difficult to compare quantitatively. Instead, three attributes were calculated from aspect imagery: north to south slope orientation (N-S; Cooper 1998), west to east slope orientation (W-E; Cooper 1998), and north-northeast to south-southwest orientation (NNE-SSW; D. W. Roberts and Cooper 1989; Table 1). Values of N-S and W-E range from -1 to 1 and represent the extent to which a slope faces north (N-S = 1), south (N-S = -1), east (W-E = 1), or west (W-E = -1). NNE-SSW represents the extent to which a slope faces the typically cooler and wetter north-northeast orientation (NNE-SSW = -1) versus the hotter and drier south-southwest orientation (NNE-SSW = 1). It has been argued that aspect should not be considered without taking into account the interactions with slope (Stage 1976). To account for this interaction, three additional attributes were calculated from the aspect and slope imagery: sine transformation (W-E A + S), cosine transformation (N-S A + S), and cosine transformation adjusted for aspect (NNE-SSW A + S). Positive values of W-E A + S are associated with east-facing slopes and negative values with west-facing slopes. For N-S A + S, positive values are north-facing slopes with negative values for south-facing slopes. N-S A + S and W-E A + S will have a zero value for pixels on flat ground, but pixels on the steep ground will have high weights for the sine and cosine of aspect. The last slope and aspect

attribute is a combination of cosine transformation and the NNE-SSW aspect attribute. The aspect was adjusted for north-northeast to south-southwest orientation, and then the cosine transformation was applied. This adjustment results in positive values being associated with north-northeast facing slopes and negative values with south-southwest facing slopes.

3. Results

Across the study region, TCI was not spatially distributed equally despite the entire region receiving similar amounts of rainfall during this period (Fig. 3). Proximity to the coast appears to result in lower TCI values, but this pattern is most likely compounded by the pattern of higher elevations also having lower TCI values. While interior areas over the Santa Ynez Mountain range experienced more elevated TCI values which was consistent across all three years and seasons. Matching the typical phenology of the region, TCI values progress throughout the season from April dates being the lowest values to August dates seeing the consistently highest TCI values across the region. Areas with typically lower TCI values, such as high-elevation areas, showed the largest increase in TCI values across the drought (Fig. 4). The largest increase in TCI was comparing August 2014 and 2015, where across the whole region there was an increase. Notably, the comparison of TCI values between 2014 and 2015 for April and June saw parts of the region, primarily interior low elevation areas, experiencing less stress despite it being a year into severe drought conditions. When comparing all pixels, so all species and landcover types, elevation presents as a strong correlating factor with TCI values (Fig. 5). However, the direction of the correlation switches between dates with April dates having a strong positive correlation and June dates having a negative correlation. The next strongest pattern of correlation across the region for topography and TCI values was aspect and slope metrics with N-S A + S and NNE-SSW A + S. South or south-southwest facing slopes were associated with high TCI values. The other terrain attributes did not have strong correlations across dates with distributions of TCI when considering the entire image.

One of the benefits of coincident hyperspectral and thermal imagery is the ability to extract plant species, which have different adaptation strategies, and be able to determine their trajectory through high-stress environmental conditions. Mediterranean grasses and forbs green up in spring, hit peak biomass in the summer, and by fall senescence. This phenology is evident in the TCI patterns, with values increasing from spring, summer, and fall imagery across 2013, 2014, and 2015 (Fig. 6). The 2015 imagery captured a shift in TCI histograms in spring and fall, with more grasses and forbs having elevated TCI values. As with patterns in correlation for the image, there are no consistent relationships between topography and TCI across the nine dates. However, elevation correlated strongest for TCI values for grasses and forbs, specifically for April 2013, November 2013, April 2014, and June 2015 dates. Slope and aspect also had a strong correlation for grasses and forbs in June 2013 and August 2014. A unique feature of an airborne dataset, compared to satellite thermal datasets, is that flightlines are collected across a time span, which gives us the opportunity to examine how TCI changes throughout the data collection. April and August 2014 had a strong correlation between time and TCI, with the progression of the day seeing increased TCI values.

Chamise is a native, dominant shrub on the landscape that is well adapted to Southern California's Mediterranean climate and burn history. Chamise is found distributed throughout this rugged terrain of the Los Padres National Forest (Fig. 3), which experienced a larger degree of change in TCI (Fig. 4). This species had a very similar distribution of TCI values in April and June across 2013, 2014, and 2015 (Fig. 6). However, the third year of the drought saw a shift in TCI values during August. TCI values correlated with slope and aspect metrics, specifically south or south-southwest-facing slopes, were associated with high TCI values for June 2013, November 2013, and August 2014 (Fig. 5). Interestingly, this association does not hold for all dates. Elevation and TCI had a strong correlation during the early dates captured of the drought, but as the drought progressed, this relationship weakened.

Coast live oak is a native, dominant tree in Southern California with adaptations such as a convex leaf shape that allow trees to survive years with limited rainfall. Coast Live Oaks are most commonly found in closer

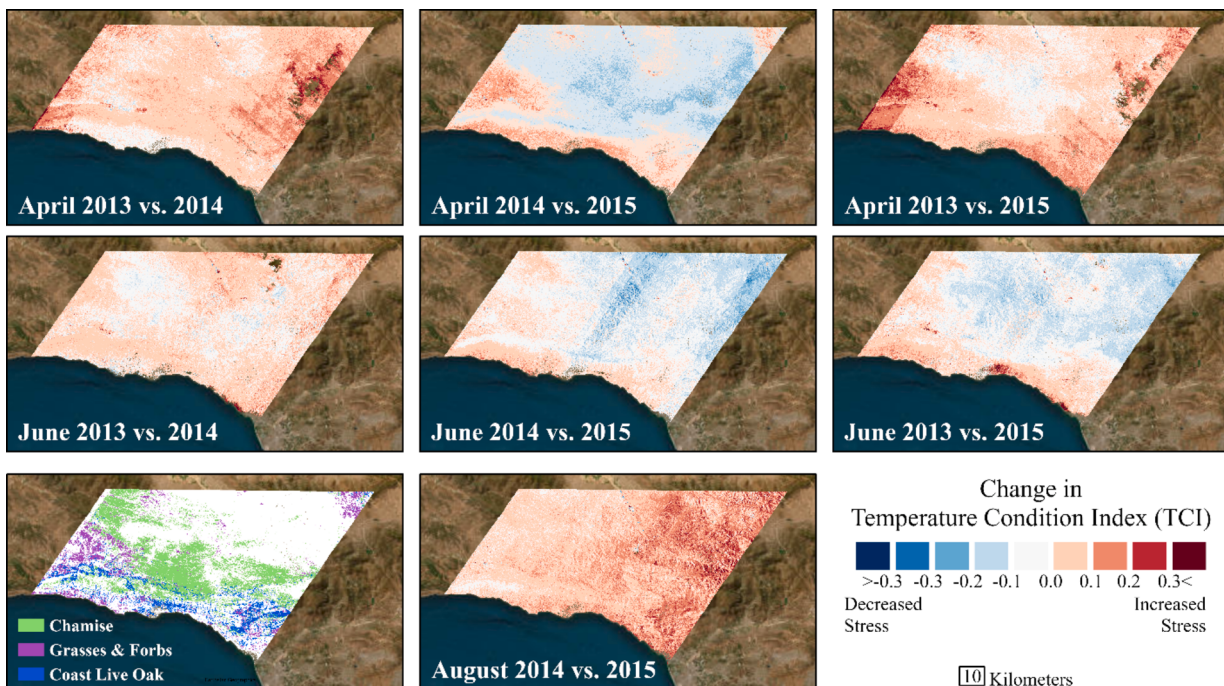


Fig. 4. Change in Temperature Condition Index (TCI) between years for spring (top row), summer (middle row), and fall (bottom row). Fall 2013 was excluded because the imagery was from November, capturing a different part of the season. In the bottom left corner is the distribution of chamise, grasses & forbs, and coast live oak determined from classifications using AVIRIS imagery, an airborne hyperspectral sensor.

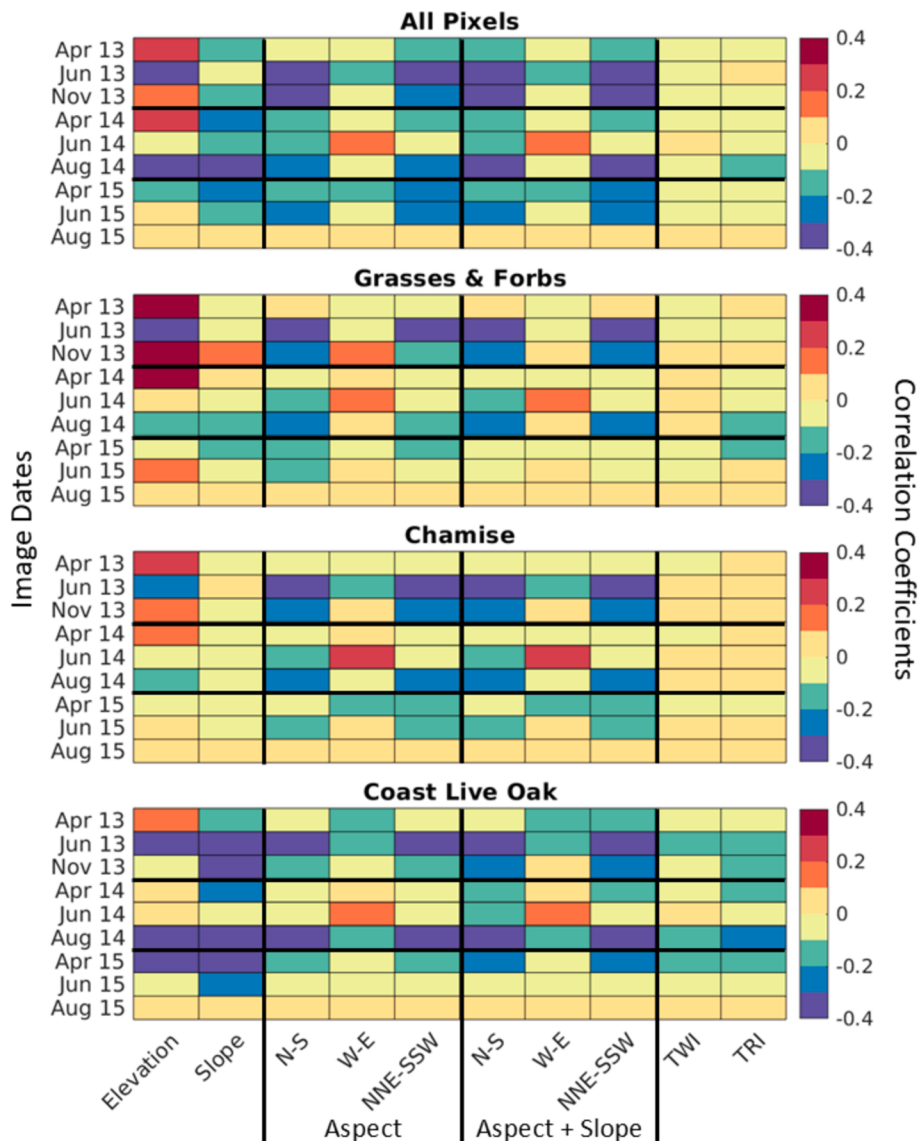


Fig. 5. The correlation between the nine image dates of Temperature Condition Index (TCI) values and topographic variables for the entire region, grasses & forbs, chamise, and coast live oak pixels (top to bottom). See Table 1 for calculations and units of topographic variables.

proximity to the coastline in the Santa Ynez Mountains, which tended to have lower TCI (Fig. 3). This species had the lowest TCI values across all seasons and years compared to the annual grasses and forbs and the chamise shrubs, but as the drought progressed, TCI values for this species did increase in April 2015 and August 2015 (Fig. 6). Coast live oak had the strongest correlations between topography and TCI values. For many dates, south or south-southwest facing slopes were associated with high TCI values. Elevation did not have as strong of a correlation as with grasses and chamise, which most likely is related to the spatial distribution of Coast Live Oak, which does not extend as far into the Los Padres National Forest.

4. Discussion

4.1. Patterns of plant species' seasonal temperature distributions

Thermal imagery has a long history of being a useful tool to gauge vegetation response to environmental conditions. In the past, these datasets were often at a coarse enough spatial resolution that it was infeasible to partition responses based on species. Even when spatial resolution would make tracking dominant species' responses across the

landscape possible, there wasn't corresponding data on species locations. With the HypsIRI airborne campaign, there is an opportunity to track species responses through coincident thermal and hyperspectral airborne imagery. In Southern California, plant species have evolved adaptations that are common in a Mediterranean climate, where precipitation is the limiting growth factor (Meentemeyer et al., 2001), and summer drought can result in 2–11 months of water deficit (Pavlik et al., 1991). In this work, we have focused on Mediterranean grasses and forbs, chamise, and coast live oak. These three species or plant communities were selected for this analysis because they have different adaptations for surviving prolonged periods of high-stress environmental conditions, which we see reflected in the TCI distributions across dates.

For Mediterranean annual grasses and forbs, the start and end of the growing season are entirely dictated by rainfall patterns (Xu and Baldocchi 2004; L. E. Jackson 1985), with peak biomass generally occurring during late spring when most of the available soil moisture has been used, followed by full senescence by late summer (Becchetti et al. 2016). These annual species have thrived in this environment in part due to their ability to exploit intermittently favorable environmental conditions for rapid plant growth (Fernández Ales, Laffarga, and Ortega

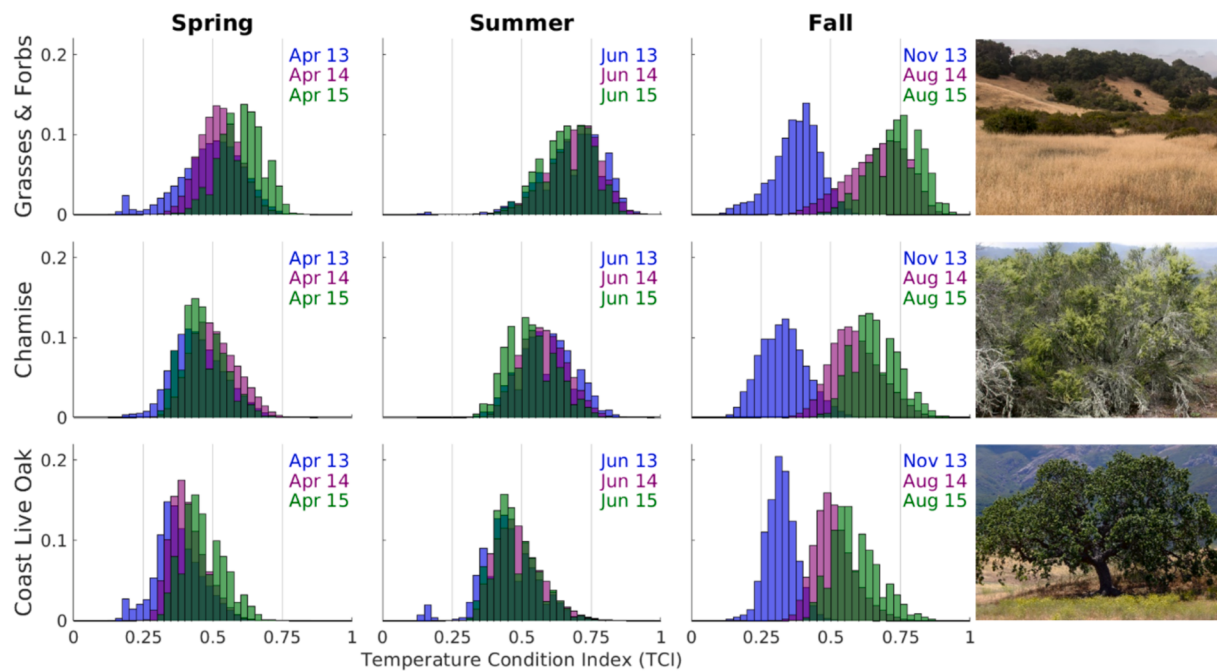


Fig. 6. Temperature condition index (TCI) histograms for all three spring dates (column 1), all three summer dates (column 2), and the two August dates (column 3) for grasses and forbs (row 1), chamise (row 2), and coast live oak (row 3) classified pixels.

1993). In this study area, TCI followed the strong phenological cycle of this vegetation community, but TCI did shift in key points of the phenology as the drought progressed, specifically in spring and fall. A longer wildfire season has been linked to increased spring temperatures (Westerling et al. 2006), and higher TCI values have implications for the impact on the beginning of the fire season (Dong et al. 2022). In actuality, the Thomas Fire initiated on December 2017 burning 281,893 acres, with a large portion of that burned area falling into this study area (CAL Fire; <https://www.fire.ca.gov/our-impact/statistics>).

Chamise is an evergreen shrub that is a characteristic species of the chaparral vegetation community. Chaparral plant species are adapted to withstand xylem cavitation and mechanical stresses that occur during the annual rainless period (Jacobsen et al. 2007). Chaparral species have key physiological adaptations that maximize the capture and utilization of water and light, which evolved as resistance to cavitation, thick evergreen leaves, and high root to shoot ratios (Kummerow, Krause, and Jow 1977; Jacobsen et al. 2007; Meentemeyer, Moody, and Franklin 2001). These adaptations translate into lower plant temperatures and less stress over the dates observed. While all chaparral species have heightened resistance, species do vary in their ability to withstand extended dry conditions by having different biomechanical properties such as stem mechanical strength, root depth, fiber properties, and post-fire regeneration (Canadell et al. 1996; Jacobsen et al. 2007). For example, chamise has a rooting depth maximum of 3.2 and 7.6 m, respectively (Canadell et al. 1996; Hellmers et al. 1955), which allows plants to access deeper water and allows them to keep stomata open, reducing plant temperatures and extending growth into the dry season (Gardner 1983). Our dataset captures this adaptation with lower overall TCI values compared to the annual grasses and forb, as well as the relative stability of those TCI values across the season. The topographic analysis confirmed that chamise shrubs experience more stress on south-southwest facing slopes, and this correlation is strongest in June and November 2013 images. During this drought, the relationship between TCI and elevation weakens during the summer and fall, suggesting that elevation is no longer a moderating influence.

Oaks are an iconic and dominant vegetation over a large part of California, and coast live oak is known for its ability to grow in drier environments than other oak species, which makes it very common in

this study area (Knops and Koenig 1994). While coast live oak is known to have a more superficial root system compared to other oak species (Cooper 1926; Barbour, Keeler-Wolf, and Schoenherr 2007), the root system is significantly more extensive than the annual Mediterranean grasses and chamise chaparral shrub examined in this work. This deeper root system corresponds to coast live oaks having larger water resources available throughout the growing season, corresponding with lower TCI values overall compared to the other species even as the growing season and drought progressed. However, in August 2015, TCI values showed an increase, which is a concern given that these slow-growing oak populations are experiencing low recruitment (Callaway and Davis 1998; Tyler, Kuhn, and Davis 2006). Summer drought was found to pose a barrier to seedling survival for coast live oak seedlings (Mahall et al. 2009). The topographic analysis confirmed that trees experience less stress at higher elevations, especially at key phenological stages in April and August in this study area, which has been linked to other tree species slowly migrating to higher elevations or northern latitudes (Lenoir et al. 2008).

4.2. Mapping plant stress

Using imagery collected over California's 2013 – 2015 drought, we used airborne thermal and hyperspectral imagery to capture plant species-specific responses to high-stress environmental conditions across the landscape. Stress was unevenly distributed across the landscape and tended to impact the very remote portions of the Los Padres National Forest that are inaccessible. August dates had elevated TCI values, especially in areas that are not accustomed to higher temperatures and lower precipitation, such as the Santa Ynez Mountains. It is worth noting that TCI is only a snapshot of a plant's current or cumulated stress, and leaf temperatures are highly influenced by the environmental conditions of that day (Gates 1968; Hamlyn G. Jones 2014). TCI is not a direct indication of repeated or cumulative stress. Plant temperature and environmental conditions have complex feedbacks as was evident with unclear or inconsistent patterns between topographic metrics and TCI. The two strongest correlating topographic factors with higher patterns of stress were lower elevations and south-southwest facing slopes, which confirms known ecological patterns.

Not only does plant stress increase a plant's susceptibility to insects and disease (Schoeneweiss 1975; R. D. Jackson 1986), but repeated water stress on plants has also been linked to an increase in fire risk for the landscape (Maselli et al. 2003; Dennison et al. 2003; Verbesselt et al. 2007). Plant stress alone is not an indication of fire risk for an area because of the complex interaction of human, ecological, and climatic factors (Vidal et al. 1994). However, this area is already prone to wildfires, with many areas burning within the last ten years (Moritz 1997). Additionally, the frequency and size of fires have been increasing in the Los Padres National Forest (Moritz 1997; Syphard, Keeley, and Brennan 2011). In our analysis, August 2015 showed the highest amount of stress across the landscape. Since June to September is the typical maximum fire danger period for this area, higher vegetation dryness due to water stress becomes a major predisposing factor for fire occurrence (Maselli et al. 2003).

Due to the increased fire risk in Mediterranean ecosystems (Mouillot, Rambal, and Joffre 2002; Fernandez-Manso, Quintano, and Roberts 2016) and the predicted increase in wildfires due to climate change (Mastrandrea and Luers 2012; Moriondo et al. 2006; Scholze et al. 2006), there has been a strong effort to predict the occurrence of wildfires. Several studies have experimentally confirmed the statistical relationship between stress indices similar to TCI and fire frequency. Using NOAA Advanced Very High-Resolution Radiometer (AVHRR) imagery, Normalized Difference Vegetation Index (NDVI) decreases in Mediterranean areas were linked to an increased probability of fire occurrence during the summer months (Maselli et al. 2003). Using Landsat imagery and an index based on the combination of vegetation index and surface minus air temperature, (Vidal and Devaux-Ros 1995) successfully located areas with high fire risk and predicted fire events. Plant stress indices, such as TCI, may provide opportunities for parameterizing climate models, fire weather monitoring, or predicting tree mortality.

4.3. Considerations when using airborne thermal imagery

An unavoidable characteristic of using large airborne thermal datasets is the temporal variation in the image collection. Throughout the day, a plant's rate of evaporation and transpiration varies (Hamlyn G. Jones and Leinonen 2003; H G Jones and Schofield 2008). It is more efficient for a plant to restrict periods of open stomata and rapid photosynthesis to those times when potential evaporation is low, particularly in the morning, and to close stomata during mid-day/afternoon, which will improve water use efficiency (Hamlyn G. Jones 2014). As stomata close and evaporation rates decrease to conserve water, a plant's leaf temperature increases (Hamlyn G. Jones and Leinonen 2003; H G Jones and Schofield 2008). Because of this relationship, diurnal patterns of plant temperatures and the difference in plant temperatures and air temperature are not static throughout the day. Plants are rarely in equilibrium with air temperature and are often warmer than the air during the day and cooler at night (Tanner 1963). This pattern is captured in diurnal patterns of latent heat flux with an increase throughout the morning and a peak around mid-day (Verma, Kim, and Clement 1989). Our analysis captured this diurnal pattern in plant temperatures and found that the timing of pixel collection was correlated with surface temperature and, ultimately, plant stress measured with TCI. Since flight lines were not all collected at the same time, patterns of plant stress captured with TCI will include hourly variability in transpiration rates.

We restricted our analysis to natural vegetation and assumed that plant species compose an entire 36 m x 36 m pixel. However, when using coarser resolution thermal imagery, the surface temperature is highly influenced by sub-pixel materials (Coates et al. 2015; Wetherley et al., 2018). The presence of soil, rock, or humanmade surfaces can be a crucial source in surface temperature variability due to material properties such as albedo, thermal conductivity, moisture content, and structure (Oke 1988). Variability within a plant species' temperature has

been found to be linked to the percent of green vegetation present in a pixel (Coates et al. 2015; D. A. Roberts et al. 2015). The Vegetation Condition Index (VCI) and Vegetation Temperature Condition (VTC) incorporate the percent green vegetation fractional cover by using the NDVI in addition to the temperature (Felix N. Kogan 1997; Singh, Roy, and Kogan 2003; Wan, Wang, and Li 2004). While NDVI has been shown to be strongly correlated with percent green vegetation, it does not directly determine the sub-pixel materials or amounts (Carlson and Ripley 1997; Montandon and Small 2008; Jiang et al. 2006). Instead, future work should incorporate percent green vegetation by using a spectral mixture analysis (Settle and Drake 1993).

The data used in this study are a precursor to the Surface Biology Geology (SBG) mission, as it was identified in the 2017 decadal survey (Cawse-Nicholson et al. 2021). The SBG mission is planning to provide hyperspectral and thermal imagery with global coverage of Earth's ecosystems every 16 days (Lee et al. 2015). Our dataset only captures a snapshot of plant stress, which is highly influenced by the environmental characteristics of that day and does not capture continued and prolonged stress throughout the year. The SBG revisit time would allow researchers to monitor yearly trends of plant stress while accounting for the daily variability seen in plants' surface temperature.

The ECOSTRESS Experiment on Space Station (ECOSTRESS) was launched in June 2018 with the primary goal of measuring plant temperatures to understand how much water plants need and how they respond to stress. The sensor was installed on the International Space Station (ISS), providing data with a 38-m in-track by 69-m cross-track spatial resolution and predicted temperature sensitivity of ≤ 0.1 K (Lee et al. 2015). With the ISS's unique orbit, composite ECOSTRESS data can be used to develop patterns of daily changes in surface temperature and evapotranspiration rates. Furthermore, the ISS orbit results in the ECOSTRESS sensor having variable revisit times, which are being used to reconstruct the daily evapotranspiration curves. Our dataset is similar to the existing ECOSTRESS data in that thermal data were collected throughout the day and not just at solar noon. These unprecedented datasets would allow for the continuous monitoring of plant stress at the species level, which can ultimately become a tool for managing natural vegetation across generally inaccessible areas or preparing and protecting communities from wildfires. Plus, predict vegetation mortality and associated changes in carbon cycling and productivity.

5. Conclusion

From 2012 to 2015, California experienced an extreme drought for which the implications are still forthcoming. What is clear is that this drought was a multimillennial-scale event whose relative severity was unprecedented. This research captured the spatial and temporal patterns of plant stress in Southern California, which can be used to help monitor and manage natural vegetation that is generally inaccessible and remote. Very few studies have been able to explore the synergies by using coincident hyperspectral and thermal imagery. These findings suggest that we can use hyperspectral and land surface temperature data to monitor plant species' response to drought conditions across the landscape. While this study used airborne data there will be an opportunity in the near future to scale this to satellite imagery using the NASA's SBG mission with a visible-shortwave infrared imaging spectrometer and thermal imager on board and has a planned launch date of April 2029. Continuing to develop and refine methods for evaluating the temporal patterns of plant species' stress is necessary for a more in-depth, quantitative understanding of the functioning natural environment. Our study takes that step, advancing our tools and understanding of how this unique dataset can monitor and ultimately provide critical information for management decisions.

CRediT authorship contribution statement

Susan K. Meerdink: Writing – review & editing, Writing – original draft, Visualization, Validation, Methodology, Formal analysis, Data curation, Conceptualization. **Dar A. Roberts:** Conceptualization, Funding acquisition, Supervision, Writing – review & editing. **Jennifer Y. King:** Writing – review & editing, Conceptualization. **Keely L. Roth:** Conceptualization. **Paul D. Gader:** Supervision, Funding acquisition, Conceptualization. **Kelly K. Caylor:** Writing – review & editing.

Declaration of competing interest

The authors declare that they have no known competing financial

interests or personal relationships that could have appeared to influence the work reported in this paper.

Acknowledgments

This project was funded as a NASA Grant NNX12AP08G, *HypIRI discrimination of plant species and functional types along a strong environmental-temperature gradient*, and a NASA Earth and Space Science Fellowship (NESSF). The project was also partially supported by the Harris Corporation.

Appendix A

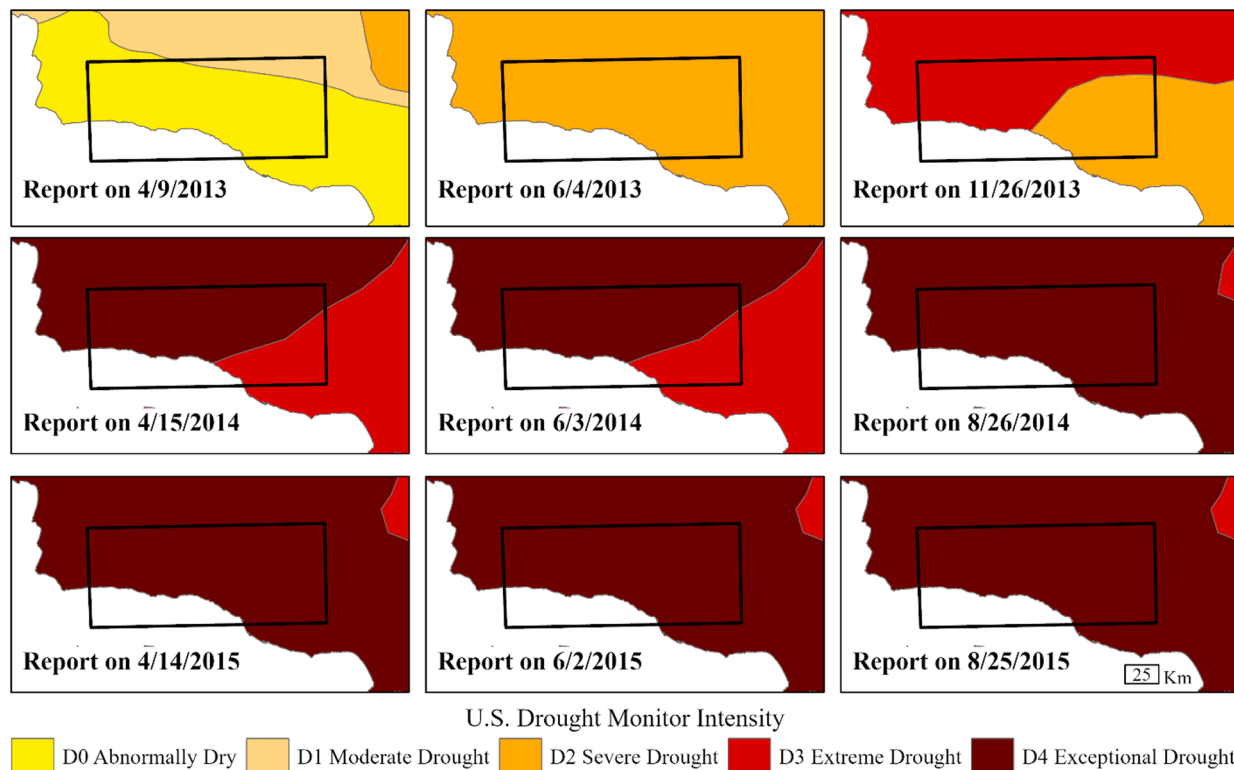


Fig. A1. The U.S. Drought Monitoring weekly reports of drought intensity rates that most closely match image dates. The study area is shown with a black outline. By August 26, 2014, the entire study area was considered as exceptional drought status.

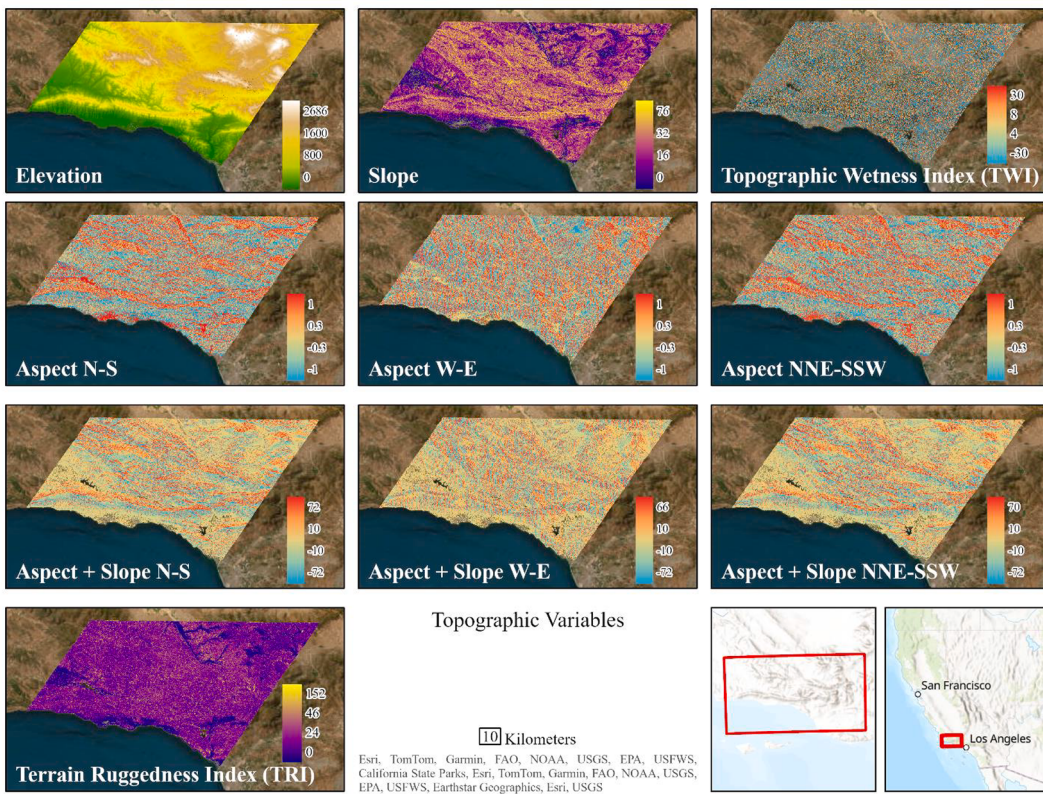


Fig. A2. The topographic variables used for correlations with the temperature condition index values.

References

- Asner, G.P., Brodrick, P.G., Anderson, C.B., Vaughn, N., Knapp, D.E., Martin, R.E., 2016. Progressive forest canopy water loss during the 2012–2015 California Drought. In: *Proceedings of the National Academy of Sciences*, p. 113 (2). <https://doi.org/10.1073/pnas.1523397113>.
- Barbour, M., Keeler-Wolf, T., Schoenherr, A.A., 2007. *Terrestrial Vegetation of California*, 3rd Edition. University of California Press.
- Bausch, W., Trout, T., Buchleiter, G., 2011. Evapotranspiration adjustments for deficit-irrigated corn using canopy temperature: a concept. *Irrig. Drain.* 60 (5), 682–693. <https://doi.org/10.1002/ird.601>.
- Bayarjargal, Y., Karnieli, A., Bayasgalan, M., Khudulmur, S., Gandush, C., Tucker, C.J., 2006. A Comparative Study of NOAA-AVHRR derived drought indices using change vector analysis. *Remote Sens. Environ.* 105 (1), 9–22. <https://doi.org/10.1016/j.rse.2006.06.003>.
- Becchetti, T., George, M., McDougald, N., Dudley, D., Connor, M., Flavel, D., Vaughn, C., et al., 2016. *Rangeland management series: annual range forage production*. University of California, Agriculture and Natural Resources. <https://doi.org/10.3733/ucanr.8018>.
- Beven, K.J., Kirby, M.J., 1979. A Physically Based, Variable Contributing Area Model of Basin Hydrology / Un Modèle à Base Physique de Zone d'appel Variable de l'hydrologie Du Bassin Versant. *Hydrol. Sci. Bull.* 24 (1), 43–69. <https://doi.org/10.1080/0262667909491834>.
- Bhuiyan, C., Singh, R.P., Kogan, F.N., 2006. Monitoring Drought Dynamics in the Aravalli Region (India) Using Different Indices Based on Ground and Remote Sensing Data. *International Journal of Applied Earth Observation and Geoinformation* 8 (4), 289–302. <https://doi.org/10.1016/j.jag.2006.03.002>.
- Blossey, B., 1999. Before, during and after: the need for long-term monitoring in invasive plant species management. *Biol. Invasions* 1 (2), 301–311. <https://doi.org/10.1023/A:1010084724526>.
- Callaway, R.M., Davis, F.W., 1998. Recruitment of *Quercus agrifolia* in Central California: the importance of shrub-dominated patches. *J. Veg. Sci.* 9 (5), 647–656. <https://doi.org/10.2307/3237283>.
- Canadell, J., Jackson, R.B., Ehleringer, J.R., Mooney, H.A., Sala, O.E., Schulze, E.-D., 1996. Maximum rooting depth of vegetation types at the global scale. *Oecologia* 108 (4), 583–595. <https://doi.org/10.1007/BF00329030>.
- Carlson, T.N., Ripley, D.A., 1997. On the Relation between NDVI, Fractional Vegetation Cover, and Leaf Area Index. *Remote Sens. Environ.* 62 (3), 241–252. [https://doi.org/10.1016/S0034-4257\(97\)00104-1](https://doi.org/10.1016/S0034-4257(97)00104-1).
- Cawse-Nicholson, K., Townsend, P.A., Schimel, D., Assiri, A.M., Blake, P.L., Buongiorno, M.F., Campbell, P., et al., 2021. NASA's surface biology and geology designated observable: a perspective on surface imaging algorithms. *Remote Sens. Environ.* 257 (May), 112349. <https://doi.org/10.1016/j.rse.2021.112349>.
- Coates, A., Dennison, P., Roberts, D., Roth, K., 2015. Monitoring the Impacts of Severe Drought on Southern California Chaparral Species Using Hyperspectral and Thermal Infrared Imagery. *Remote Sens. (Basel)* 7 (11), 14276–14291. <https://doi.org/10.3390/rs71114276>.
- Cooper, W.S., 1926. Vegetational Development Upon Alluvial Fans in The Vicinity of Palo Alto, California. *Ecology* 7 (1), 1–30. <https://doi.org/10.2307/1929116>.
- Cooper. 1998. "The Use of Terrain Analysis in the Evaluation of Snow Cover over an Alpine Glacier." In *Landform Monitoring, Modelling and Analysis*. New York, NY, USA. <https://www.wiley.com/en-gb/Landform+Monitoring%2C+Modelling+and+Analysis-p-9780471969778>.
- Davis, F.W., Michaelsen, J., 1995. Sensitivity of Fire Regime in Chaparral Ecosystems to Climate Change. In: Moreno, J.M., Oechel, W.C. (Eds.), *Global Change and Mediterranean-Type Ecosystems*. Springer, New York, NY, pp. 435–456. https://doi.org/10.1007/978-1-4612-4186-7_21.
- Dennison, P.E., Roberts, D.A., Thorngren, S.R., Regelbrugge, J.C., Weise, D., Lee, C., 2003. Modeling Seasonal Changes in Live Fuel Moisture and Equivalent Water Thickness Using a Cumulative Water Balance Index. *Remote Sens. Environ.* 88 (4), 442–452. <https://doi.org/10.1016/j.rse.2003.08.015>.
- Diamond, H.J., Karl, T.R., Palecki, M.A., Bruce Baker, C., Bell, J.E., Leeper, R.D., Easterling, D.R., et al., 2013. U.S. Climate Reference Network after One Decade of Operations: Status and Assessment. *Bull. Am. Meteorol. Soc.* 94 (4), 485–498. <https://doi.org/10.1175/BAMS-D-12-00170.1>.
- Dong, C., Park Williams, A., Abatzoglou, J.T., Lin, K., Okin, G.S., Gillespie, T.W., Long, D. i., Lin, Y.-H., Hall, A., MacDonald, G.M., 2022. The Season for Large Fires in Southern California Is Projected to Lengthen in a Changing Climate. *Commun. Earth Environ.* 3 (1), 1–9. <https://doi.org/10.1038/s43247-022-00344-6>.
- Fernández Ales, R., Laffarga, J.M., Ortega, F., 1993. Strategies in Mediterranean Grassland Annuals in Relation to Stress and Disturbance. *J. Veg. Sci.* 4 (3), 313–322. <https://doi.org/10.2307/3235589>.
- Fernandez-Manso, A., Quintano, C., Roberts, D.A., 2016. Burn Severity Influence on Post-Fire Vegetation Cover Resilience from Landsat MESMA Fraction Images Time Series in Mediterranean Forest Ecosystems. *Remote Sens. Environ.* 184 (October), 112–123. <https://doi.org/10.1016/j.rse.2016.06.015>.
- Gardner, W.R., 1983. Soil Properties and Efficient Water Use: An Overview. In: *Limitations to Efficient Water Use in Crop Production*. John Wiley & Sons, Ltd, pp. 45–64. <https://doi.org/10.2134/1983.limitationstoefficientwateruse.c3>.
- Gates, D. M. 1968. "Transpiration and Leaf Temperature." *Annual Review of Plant Biology* 19 (Volume 19, 1968): 211–38. DOI: 10.1146/annurev.pp.19.06168.001235.
- Gillespie, A., Rokugawa, S., Matsunaga, T., Cothren, J.S., Hook, S., Kahle, A.B., 1998. A Temperature and Emissivity Separation Algorithm for Advanced Spaceborne

- Thermal Emission and Reflection Radiometer (ASTER) Images. *IEEE Trans. Geosci. Remote Sens.* 36 (4), 1113–1126. <https://doi.org/10.1109/36.700995>.
- Green, R.O., Eastwood, M.L., Sarture, C.M., Chrien, T.G., Aronsson, M., Chippendale, B.J., Faust, J.A., et al., 1998. Imaging Spectroscopy and the Airborne Visible/Infrared Imaging Spectrometer (AVIRIS). *Remote Sens. Environ.* 65 (3), 227–248. [https://doi.org/10.1016/S0034-4257\(98\)00064-9](https://doi.org/10.1016/S0034-4257(98)00064-9).
- Griffin, D., Anchukaitis, K.J., 2014. How Unusual Is the 2012–2014 California Drought? *Geophys. Res. Lett.* 41 (24), 9017–9023. <https://doi.org/10.1002/2014GL062433>.
- Guarín, A., Taylor, A.H., 2005. Drought Triggered Tree Mortality in Mixed Conifer Forests in Yosemite National Park, California, USA. *For. Ecol. Manage.* 218 (1), 229–244. <https://doi.org/10.1016/j.foreco.2005.07.014>.
- Hellmers, H., Horton, J.S., Juhren, G., O'Keefe, J., 1955. Root Systems of Some Chaparral Plants in Southern California. *Ecology* 36 (4), 667–678. <https://doi.org/10.2307/1931305>.
- Hook, S.J., Myers, J.J., Thome, K.J., Fitzgerald, M., Kahle, A.B., 2001. The MODIS/ASTER Airborne Simulator (MASTER) — A New Instrument for Earth Science Studies. *Remote Sens. Environ.* 76 (1), 93–102.
- Hulley, G.C., Hook, S.J., 2011. Generating Consistent Land Surface Temperature and Emissivity Products Between ASTER and MODIS Data for Earth Science Research. *IEEE Trans. Geosci. Remote Sens.* 49 (4), 1304–1315. <https://doi.org/10.1109/TGRS.2010.2063034>.
- Idso, S.B., Jackson, R.D., Pinter, P.J., Reginato, R.J., Hatfield, J.L., 1981. Normalizing the Stress-Degree-Day Parameter for Environmental Variability. *Agric. Meteorol.* 24 (January), 45–55. [https://doi.org/10.1016/0002-1571\(81\)90032-7](https://doi.org/10.1016/0002-1571(81)90032-7).
- Jackson, L.E., 1985. Ecological Origins of California's Mediterranean Grasses. *J. Biogeogr.* 12 (4), 349–361. <https://doi.org/10.2307/2844866>.
- Jackson, R.D., 1986. Remote Sensing of Biotic and Abiotic Plant Stress. *Annu. Rev. Phytopathol.* 24 (1), 265–287. <https://doi.org/10.1146/annurev.py.24.090186.001405>.
- Jackson, R.D., Reginato, R.J., Idso, S.B., 1977. Wheat Canopy Temperature: A Practical Tool for Evaluating Water Requirements. *Water Resour. Res.* 13 (3), 651–666.
- Jackson, R.D., Idso, S.B., Reginato, R.J., Pinter Jr., P.J., 1981. Canopy Temperature as a Crop Water Stress Indicator. *Water Resour. Res.* 17 (4), 1133–2118. <https://doi.org/10.1029/WR017004p01133>.
- Jacobsen, A.L., Brandon Pratt, R., Ewers, F.W., Davis, S.D., 2007. Cavitation Resistance Among 26 Chaparral Species of Southern California. *Ecol. Monogr.* 77 (1), 99–115. <https://doi.org/10.1890/05-1879>.
- Jiang, Z., Huete, A.R., Chen, J., Chen, Y., Li, J., Yan, G., Zhang, X., 2006. Analysis of NDVI and Scaled Difference Vegetation Index Retrievals of Vegetation Fraction. *Remote Sens. Environ.* 101 (3), 366–378. <https://doi.org/10.1016/j.rse.2006.01.003>.
- Jones, H.G., 2014. *Plants and Microclimate: A Quantitative Approach to Environmental Plant Physiology*, 3rd edition. Cambridge University Press, Cambridge (GB).
- Jones, H.G., Leinonen, I., 2003. Thermal Imaging for the Study of Plant Water Relations. *Journal of Agriculture Meteorology* 59 (3), 205–217.
- Jones, H.G., Schofield, P., 2008. Thermal and Other Remote Sensing of Plant Stress. *General Applied Plant Physiology* 34 (1–2), 19–32.
- Karniel, A., Bayasgalan, M., Bayarjargal, Y., Agam, N., Khudulmur, S., Tucker, C.J., 2006. Comments on the Use of the Vegetation Health Index over Mongolia. *Int. J. Remote Sens.* 27 (10), 2017–2024. <https://doi.org/10.1080/01431160500121727>.
- Knops, J.M.H., Koenig, W.D., 1994. Water Use Strategies of Five Sympatric Species of *Quercus* in Central Coastal California. *Madroño* 41 (4), 290–301.
- Kogan, F.N., 1995. Application of Vegetation Index and Brightness Temperature for Drought Detection. *Adv. Space Res.*, Natural Hazards: Monitoring and Assessment Using Remote Sensing Technique 15 (11), 91–100. [https://doi.org/10.1016/0273-1177\(95\)00079-T](https://doi.org/10.1016/0273-1177(95)00079-T).
- Kogan, F.N., 1997. Global Drought Watch from Space. *Bull. Am. Meteorol. Soc.* 78 (4), 621–636. [https://doi.org/10.1175/1520-0477\(1997\)078-0621:GDWFS>2.0.CO;2](https://doi.org/10.1175/1520-0477(1997)078-0621:GDWFS>2.0.CO;2).
- Kogan, F., Stark, R., Gitelson, A., Jargalsaikhan, L., Dugraja, C., Tssooj, S., 2004. Derivation of Pasture Biomass in Mongolia from AVHRR-Based Vegetation Health Indices. *Int. J. Remote Sens.* 25 (14), 2889–2896. <https://doi.org/10.1080/01431160410001697619>.
- Kummerow, J., Krause, D., Jow, W., 1977. Root Systems of Chaparral Shrubs. *Oecologia* 29 (2), 163–177. <https://doi.org/10.1007/BF00345795>.
- Ustin, Daniel J. Mandl, and Elizabeth M. Middleton. 2015. "An Introduction to the NASA Hyperspectral InfraRed Imager (HypIRI) Mission and Preparatory Activities." *Remote Sensing of Environment*, Special Issue on the Hyperspectral Infrared Imager (HypIRI), 167 (September):6–19. DOI: 10.1016/j.rse.2015.06.012.
- Lenoir, J., Gégoût, J.C., Marquet, P.A., de Ruffray, P., Brisse, H., 2008. A Significant Upward Shift in Plant Species Optimum Elevation During the 20th Century. *Science* 320 (5884), 1768–1771. <https://doi.org/10.1126/science.1156831>.
- Mahall, B.E., Tyler, C.M., Shelly Cole, E., Mata, C., 2009. A Comparative Study of Oak (*Quercus*, Fagaceae) Seedling Physiology during Summer Drought in Southern California. *Am. J. Bot.* 96 (4), 751–761. <https://doi.org/10.3732/ajb.0800247>.
- Mann, M.E., Gleick, P.H., 2015. Climate Change and California Drought in the 21st Century. *Proc. Natl. Acad. Sci.* 112 (13), 3858–13389. <https://doi.org/10.1073/pnas.1503667112>.
- Maselli, F., Romanelli, S., Bottai, L., Zipoli, G., 2003. Use of NOAA-AVHRR NDVI Images for the Estimation of Dynamic Fire Risk in Mediterranean Areas. *Remote Sens. Environ.* 86 (2), 187–197. [https://doi.org/10.1016/S0034-4257\(03\)00099-3](https://doi.org/10.1016/S0034-4257(03)00099-3).
- Mastrandrea, M.D., Luers, A.L., 2012. Climate Change in California: Scenarios and Approaches for Adaptation. *Clim. Change* 111 (1), 5–16. <https://doi.org/10.1007/s10584-011-0240-4>.
- Mastrandrea, M.D., Tebaldi, C., Snyder, C.W., Schneider, S.H., 2011. Current and Future Impacts of Extreme Events in California. *Clim. Change* 109 (1), 43–70. <https://doi.org/10.1007/s10584-011-0311-6>.
- McNab, W. Henry, and Peter E. Avers. 1996. "Ecological Subregions of the United States." WO-WSA-5. USDA Forest Service. <https://www.fs.usda.gov/land/pubs/ecoregions/>.
- Meentemeyer, R.K., Moody, A., Franklin, J., 2001. Landscape-Scale Patterns of Shrub-Species Abundance in California Chaparral – The Role of Topographically Mediated Resource Gradients. *Plant Ecol.* 156 (1), 19–41. <https://doi.org/10.1023/A:1011944805738>.
- Meerdink, S.K., Roberts, D.A., King, J.Y., Roth, K.L., Dennison, P.E., Amaral, C.H., Hook, S.J., 2016. Linking Seasonal Foliar Traits to VSWIR-TIR Spectroscopy across California Ecosystems. *Remote Sens. Environ.* 186 (December), 322–338. <https://doi.org/10.1016/j.rse.2016.08.003>.
- Meerdink, S.K., Roberts, D.A., Roth, K.L., King, J.Y., Gader, P.D., Koltunov, A., 2019. Classifying California Plant Species Temporally Using Airborne Hyperspectral Imagery. *Remote Sens. Environ.* 232 (October), 111308. <https://doi.org/10.1016/j.rse.2019.111308>.
- Montandon, L.M., Small, E.E., 2008. The Impact of Soil Reflectance on the Quantification of the Green Vegetation Fraction from NDVI - ScienceDirect. *Remote Sens. Environ.* 112 (4), 1835–1845. <https://doi.org/10.1016/j.rse.2007.09.007>.
- Moran, M.S., Clarke, T.R., Inoue, Y., Vidal, A., 1994. Estimating Crop Water Deficit Using the Relation between Surface-Air Temperature and Spectral Vegetation Index. *Remote Sens. Environ.* 49 (3), 246–263. [https://doi.org/10.1016/0034-4257\(94\)90020-5](https://doi.org/10.1016/0034-4257(94)90020-5).
- Moreno, J.M., Oechel, W.C., 1991. Fire Intensity and Herbivory Effects on Postfire Resprouting of Adenostoma fasciculatum in Southern California Chaparral. *Oecologia* 85 (3), 429–433. <https://doi.org/10.1007/BF00320621>.
- Moriondo, M., Good, P., Durao, R., Bindi, M., Giannakopoulos, C., Corte-Real, J., 2006. Potential Impact of Climate Change on Fire Risk in the Mediterranean Area. *Climate Res.* 31 (1), 85–95. <https://doi.org/10.3354/cr031085>.
- Moritz, M.A., 1997. Analyzing Extreme Disturbance Events: Fire in Los Padres National Forest. *Ecol. Appl.* 7 (4), 1252–1262. [https://doi.org/10.1890/1051-0761\(1997\)007\[1252:ADEFIJ\]2.0.CO;2](https://doi.org/10.1890/1051-0761(1997)007[1252:ADEFIJ]2.0.CO;2).
- Mouillot, F., Rambal, S., Joffre, R., 2002. Simulating Climate Change Impacts on Fire Frequency and Vegetation Dynamics in a Mediterranean-Type Ecosystem. *Glob. Chang. Biol.* 8 (5), 423–437. <https://doi.org/10.1046/j.1365-2486.2002.00494.x>.
- Nichol, J.E., Abbas, S., 2015. Integration of Remote Sensing Datasets for Local Scale Assessment and Prediction of Drought. *Science of the Total Environment* 505 (February), 503–507. <https://doi.org/10.1016/j.scitotenv.2014.09.099>.
- Oke, T.R., 1988. The Urban Energy Balance. *Prog. Phys. Geogr.: Earth Environ.* 12 (4), 471–508. <https://doi.org/10.1177/03091338801200401>.
- Pavlik, B.M., Muick, P., Johnson, S., 1991. *Oaks of California*. 2nd, Printing edition. Cachuma Pr, Los Olivos, CA.
- Riley, S.J., DeGloria, S.D., Elliot, R., 1999. A Terrian Ruggedness Index That Quantifies Topographic Heterogeneity. *Intermountain Journal of Sciences* 5, 1–4.
- Roberts, D.W., Cooper, S.V., 1989. Concepts and Techniques of Vegetation Mapping. U.S. Department of Agriculture, Intermountain Forest and Range Experiment Station, Forest Service.
- Roberts, D.A., Dennison, P.E., Roth, K.L., Dudley, K., Hulley, G., 2015. Relationships between Dominant Plant Species, Fractional Cover and Land Surface Temperature in a Mediterranean Ecosystem. *Remote Sens. Environ.* 167 (September), 152–167. <https://doi.org/10.1016/j.rse.2015.01.026>.
- Schoeneweis, D.F., 1975. Predisposition, Stress, and Plant Disease. *Annu. Rev. Phytopathol.* no. 31.
- Scholze, M., Knorr, W., Arnell, N.W., Colin Prentice, I., 2006. A Climate-Change Risk Analysis for World Ecosystems. *Proc. Natl. Acad. Sci.* 103 (35), 13116–13120. <https://doi.org/10.1073/pnas.0601816103>.
- Settle, J.J., Drake, N.A., 1993. Linear Mixing and the Estimation of Ground Cover Proportions. *Int. J. Remote Sens.* 14 (6), 1159–1177. <https://doi.org/10.1080/01431169308904402>.
- Singh, R.P., Roy, S., Kogan, F., 2003. Vegetation and Temperature Condition Indices from NOAA AVHRR Data for Drought Monitoring over India. *Int. J. Remote Sens.* 24 (22), 4393–4402. <https://doi.org/10.1080/0143116031000084323>.
- Stage, A.R., 1976. An Expression for the Effect of Aspect, Slope, and Habitat Type on Tree Growth. *For. Sci.* 22 (4), 457–460.
- Swain, D.I., 2014. The Extraordinary California Drought of 2013/2014: Character, Context, and the Role of Climate Change. *Bull. Am. Meteorol. Soc.* 95 (9).
- Syphard, A.D., Keeley, J.E., Brennan, T.J., 2011. Factors Affecting Fuel Break Effectiveness in the Control of Large Fires on the Los Padres National Forest, California. *Int. J. Wildland Fire* 20 (6), 764–775. <https://doi.org/10.1071/WF10065>.
- Taghvaeian, S., Comas, L., DeJonge, K.C., Trout, T.J., 2014. Conventional and Simplified Canopy Temperature Indices Predict Water Stress in Sunflower. *Agric. Water Manag.* 144 (October), 69–80.
- Taiwo, Balogun Emmanuel, Abdulla - Al Kafy, Ajeyomi Adedoyin Samuel, Zulayyadini A. Rahaman, Ologun Emmanuel Ayowole, Mahir Shahrier, Bushra Monowar Duti, Muhammad Tauhidur Rahman, Olarewaju Timilehin Peter, and Olamijju Oluyinka Abosede. 2023. "Monitoring and Predicting the Influences of Land Use/Land Cover Change on Cropland Characteristics and Drought Severity Using Remote Sensing Techniques." *Environmental and Sustainability Indicators* 18 (June):100248. DOI: 10.1016/j.indic.2023.100248.
- Tane, Z., Roberts, D., Koltunov, A., Sweeney, S., Ramirez, C., 2018. A Framework for Detecting Conifer Mortality across an Ecoregion Using High Spatial Resolution Spaceborne Imaging Spectroscopy. *Remote Sens. Environ.* 209 (May), 195–210. <https://doi.org/10.1016/j.rse.2018.02.073>.
- Tanner, C.B., 1963. Plant Temperatures. *Agron. J.* 55 (2), 210–221. <https://doi.org/10.2134/agronj1963.00021962005500020043x>.
- Thompson, David R., Bo-Cai Gao, Robert O. Green, Dar A. Roberts, Philip E. Dennison, and Sarah R. Lundeen. 2015. "Atmospheric Correction for Global Mapping

- Spectroscopy: ATREM Advances for the HypsIRI Preparatory Campaign." *Remote Sensing of Environment*, Special Issue on the Hyperspectral Infrared Imager (HypsIRI), 167 (September):64–77. DOI: 10.1016/j.rse.2015.02.010.
- Thomson, S., Ouellet-Plamondon, C., DeFauw, S., Huang, Y., Fisher, D., English, P., 2012. Potential and Challenges in Use of Thermal Imaging for Humid Region Irrigation System Management. *J. Agric. Sci.* 4 (4), p103. <https://doi.org/10.5539/jas.v4n4p103>.
- Tyler, C.M., Kuhn, B., Davis, F.W., 2006. Demography and Recruitment Limitations of Three Oak Species in California. *Q. Rev. Biol.* 81 (2), 127–152. <https://doi.org/10.1086/506025>.
- Verbesselt, J., Somers, B., Lhermitte, S., Jonckheere, I., van Aardt, J., Coppin, P., 2007. Monitoring Herbaceous Fuel Moisture Content with SPOT VEGETATION Time-Series for Fire Risk Prediction in Savanna Ecosystems. *Remote Sens. Environ.* 108 (4), 357–368. <https://doi.org/10.1016/j.rse.2006.11.019>.
- Verma, S.B., Kim, J., Clement, R.J., 1989. Carbon Dioxide, Water Vapor and Sensible Heat Fluxes over a Tallgrass Prairie. *Bound.-Lay. Meteorol.* 46 (1), 53–67. <https://doi.org/10.1007/BF00118446>.
- Vidal, A., Devaux-Ros, C., 1995. Evaluating Forest Fire Hazard with a Landsat TM Derived Water Stress Index. *Agric. For. Meteorol.*, Thermal Remote Sensing of the Energy and Water Balance over Vegetation 77 (3), 207–224. [https://doi.org/10.1016/0168-1923\(95\)02262-V](https://doi.org/10.1016/0168-1923(95)02262-V).
- Vidal, A., Pinglo, F., Durand, H., Devaux-Ros, C., Maillet, A., 1994. Evaluation of a Temporal Fire Risk Index in Mediterranean Forests from NOAA Thermal IR. *Remote Sens. Environ.* 49 (3), 296–303. [https://doi.org/10.1016/0034-4257\(94\)90024-8](https://doi.org/10.1016/0034-4257(94)90024-8).
- Wan, Z., Wang, P., Li, X., 2004. Using MODIS Land Surface Temperature and Normalized Difference Vegetation Index Products for Monitoring Drought in the Southern Great Plains, USA. *Int. J. Remote Sens.* 25 (1), 61–72. <https://doi.org/10.1080/0143116031000115328>.
- Westerling, A.L., Hidalgo, H.G., Cayan, D.R., Swetnam, T.W., 2006. Warming and Earlier Spring Increase Western U.S. Forest Wildfire Activity. *Science* 313 (5789), 940–993. <https://doi.org/10.1126/science.1128834>.
- Wetherley, E.B., McFadden, J.P., Roberts, D.A., 2018. Megacity-Scale Analysis of Urban Vegetation Temperatures. *Remote Sens. Environ.* 213 (August), 18–33. <https://doi.org/10.1016/j.rse.2018.04.051>.
- Xu, L., Baldocchi, D.D., 2004. Seasonal Variation in Carbon Dioxide Exchange over a Mediterranean Annual Grassland in California. *Agric. For. Meteorol.* 123 (1), 79–96. <https://doi.org/10.1016/j.agrformet.2003.10.004>.
- Young, D.J.N., Stevens, J.T., Mason Earles, J., Moore, J., Ellis, A., Jirka, A.L., Latimer, A. M., 2017. Long-term climate and competition explain forest mortality patterns under extreme drought. *Ecol. Lett.* 20 (1), 78–86. <https://doi.org/10.1111/ele.12711>.
- Zhai, H., Zhang, H., Zhang, L., Li, P., 2018. Cloud/shadow detection based on spectral indices for multi/hyperspectral optical remote sensing imagery. *ISPRS J. Photogramm. Remote Sens.* 144 (October), 235–253. <https://doi.org/10.1016/j.isprsjprs.2018.07.006>.